Nano Energy 28 (2016) 143–150

Contents lists available at ScienceDirect

Nano Energy

journal homepage: www.elsevier.com/locate/nanoen

$CoSe_2$ nanoparticles embedded defective carbon nanotubes derived from MOFs as efficient electrocatalyst for hydrogen evolution reaction

Weijia Zhou [a,b,*,1], Jia Lu [a,1], Kai Zhou [a], Linjing Yang [a], Yunting Ke [a], Zhenghua Tang [a,b], Shaowei Chen [a,c,*]

[a] New Energy Research Institute, School of Environment and Energy, South China University of Technology, Guangzhou Higher Education Mega Center, Guangzhou, Guangdong 510006, China
[b] Guangdong Provincial Key Laboratory of Atmospheric Environment and Pollution Control, South China University of Technology, Guangzhou Higher Education Mega Centre, Guangzhou 510006, China
[c] Department of Chemistry and Biochemistry, University of California, 1156 High Street, Santa Cruz, CA 95064, United States

ARTICLE INFO

Article history:
Received 21 April 2016
Received in revised form
4 August 2016
Accepted 17 August 2016
Available online 17 August 2016

Keywords:
Core-shell structure
Metal-organic framework
Carbon nanotube
Pre-oxidation
Hydrogen evolution reaction

ABSTRACT

Development of electrocatalysts for hydrogen evolution reaction (HER) with low overpotential and robust stability remained as one of the most serious challenges for energy conversion. In this work, $CoSe_2$ nanoparticles embedded in defective carbon nanotubes ($CoSe_2$@DC) was synthesized by a carbonization-oxidation-selenylation procedure of Co-based metal-organic frameworks (MOFs). The pre-oxidation treatment was a crucial step in introducing an increasing number of defects into carbon nanotubes, which promoted the reaction between Co@carbon and selenium and led to the enhanced HER performance. The as-prepared $CoSe_2$@DC exhibited excellent HER catalytic reactivity with a low onset potential of -40 mV vs. RHE, a small Tafel slope of 82 mV dec^{-1} as well as a high current density with robust catalytic stability in 0.5 M H_2SO_4. This work may provide a generic methodology for rational design and fabrication of the partially encased core-shell structure derived from MOFs as efficient HER electrocatalysts.

1. Introduction

Hydrogen is considered as one of the promising alternatives for replacing fossil fuels due to their high energy density and environmental friendliness. Electrochemical water splitting is one of the clean and efficient methods to produce molecular hydrogen in large quantity. To date, platinum-based materials are the most efficient catalysts for hydrogen evolution reaction (HER), but the high cost and low abundance significantly hamper their widespread applications [1,2]. Thus, a great deal of research efforts have been devoted to develop low-cost and earth-abundant catalysts to replace Pt-based catalysts [3,4]. One is the transition-metal based catalysts, including its chalcogenides [5,6], carbides [7,8], phosphides [2,9,10] and nitrides [11,12]. The other is carbon-based catalysts, nonmetal doped carbon (N, S, P) [13–15] and metal@carbons (Fe, Co and alloy@C) [16–18]. However, how to combine the high catalytic activity of transition metals and the great stability of carbon is still an urgent task in promoting water splitting catalysis.

Metal-organic frameworks (MOFs) with diverse composition and controllable porous structures are assembled by metal ions as nodes and organic ligands as struts through coordination bonds [19,20]. MOFs as both templates and precursors can be used to synthesize functional carbon-wrapped metal nanoparticles via direct pyrolysis under an inert atmosphere [15,18,21], and several hybrid materials derived from MOFs have been employed as efficient HER electrocatalysts [22–24]. For instance, Wen and Chen et al. [25] synthesized a complicated hybrid electrocatalyst consisting of N-doped graphene/cobalt embedded porous carbon by pyrolysis of graphene oxide-supported Co-MOFs, which showed apparent HER activity with an onset potential of -58 mV vs. RHE and a stable current density of 10 mA cm^{-2} at 229 mV in acid media. The theoretical calculation confirmed that the ultrathin graphene shells, which should less than 2 nm, strongly promoted electron penetration from the metal core to the graphene surface to enhance HER activity. However, the thickness of carbon shell was difficult to be controlled in the preparation of metal@carbon. If the carbon shells were too thick (more than 2 nm), the catalytic activities of metal@carbon electrocatalysts were weakened. In

* Corresponding authors at: New Energy Research Institute, School of Environment and Energy, South China University of Technology, Guangzhou Higher Education Mega Center, Guangzhou, Guangdong 510006, China.
E-mail addresses: eszhouwj@scut.edu.cn (W. Zhou), shaowei@ucsc.edu (S. Chen).
[1] These authors contributed equally to the work.

http://dx.doi.org/10.1016/j.nanoen.2016.08.040
2211-2855/

order to solve the above problems, the etching process of metal@carbon by pre-oxidation was employed. Herein, metal compound@carbon hybrids, such as $CoSe_2$ nanoparticles embedded defective carbon ($CoSe_2$@DC) derived from Co-based MOFs, have been synthesized for HER. $CoSe_2$ is a kind of efficient catalysts for HER [17,26]. Herein, benefiting from the synergic effect between a $CoSe_2$ core and a defective carbon shell, the as-prepared $CoSe_2$@DC exhibited excellent HER activity with a low onset potential of -40 mV vs. RHE, a Tafel slope of 82 mV dec^{-1} as well as a high current density with robust catalytic stability in 0.5 M H_2SO_4.

2. Experimental section

2.1. Chemicals

All reagents were of analytical grade and used without further purification. Cobalt nitrate hexahydrate ($Co(NO_3)_2 \cdot 6H_2O$), cobalt acetate tetrahydrate ($C_2H_3CoO_2 \cdot 4H_2O$), 2-methylimidazole ($C_4H_6N_2$), selenium powder (Se), selenium dioxide (SeO_2) powder, sulfuric acid (H_2SO_4), methanol, ethanediamine, dicyandiamide, carbon nanotubes and 20 wt% Pt/C were purchased from Sinopharm Chemical Reagents Beijing Co. and used as received.

2.2. Synthesis of $CoSe_2$ nanoparticles embedded defective carbon ($CoSe_2$@DC)

ZIF-67 metal organic framework (Co based MOFs) were prepared according to a previous report [27]. Then, the prepared ZIF-67 samples were transferred to a furnace tube and pyrolyzed under an Ar atmosphere at 800 °C for 2 h. The resulting product was dispersed in 0.5 M H_2SO_4 overnight to remove residual metallic cobalt to obtain Co nanoparticles embedded carbon nanotubes (Co@C). Subsequently, the Co@C powders were transferred into a muffle furnace and heated at 350 °C for 2 h in air to synthesize Co_3O_4 nanoparticles embedded defective carbon nanotubes (Co_3O_4@DC). Finally, the Co_3O_4@DC powders were put into the center of a tube furnace, and selenium powders were placed at the upstream side of the furnace. The center of the furnace was quickly heated up to 450 °C in 20 min under an Ar atmosphere and kept for 30 min, the as-obtained product were denoted as $CoSe_2$@DC. For comparison, composites were also synthesized by the same procedures but without the oxidation step, which was denoted as Co@C-Se.

2.3. Synthesis of pure $CoSe_2$

0.6 g $C_2H_3CoO_2 \cdot 4H_2O$ were placed into a crucible and then put into the center of a tube furnace. The subsequent selenylation process was the same as for $CoSe_2$@DC. The resulting product was dispersed in 0.5 M H_2SO_4 overnight and then filtered and washed several times with deionized water to finally obtain the $CoSe_2$ product.

2.4. Synthesis of defective carbon (DC)

The synthetic process of defective carbon (DC) was similar to that for $CoSe_2$@DC, except for using ZIF-8 (Zn based MOFs) as the precursor instead of ZIF-67 (Co based MOFs). The XRD patterns of ZIF-67 and ZIF-8 were shown in Fig. S1, which confirmed the successful synthesis of MOFs.

2.5. Synthesis of $CoSe_2$ nanoparticles loaded defective carbon nanotubes ($CoSe_2$/DC)

Prior to the synthesis of $CoSe_2$/DC, the defective carbon nanotubes were prepared by calcining carbon nanotubes in air at 350 °C for 2 h. Typically, for the synthesis of $CoSe_2$/DC, 1.2 mmol $C_2H_3CoO_2 \cdot 4H_2O$, 4.8 mmol SeO_2 powders and 300 mg DC were dissolved in 10 mL deionized water under magnetic stirring and then sonicated for 30 min to form a homogeneous solution. Then, 25 mL ethanediamine was added under continuous stirring for another 15 min, and the final solution was transferred into a 40 mL Teflon-lined stainless steel autoclave and kept at 200 °C for 20 h. The obtained black products were washed by deionized water for at least 3 times, collected by centrifugation and dried at 60 °C in air. Finally, the dried samples were annealed at 500 °C for 1 h under a N_2 atmosphere to obtain $CoSe_2$/DC.

2.6. Characterization

Field-emission scanning electron microscopic (FESEM, NOVA NANOSEM 430, FEI) measurements were employed to characterize the morphologies of the as-prepared samples. Transmission electron microscopic (TEM) measurements were carried out with a Tecnai G220 FEI microscope. Powder X-ray diffraction (XRD) patterns of the samples were recorded on a Bruker D8 Advance powder X-ray diffractometer with Cu Kα ($\lambda = 0.15406$ nm) radiation. X-ray photoelectron spectroscopic (XPS) measurements were performed using a PHI X-tool instrument. Raman spectra were acquired on a RENISHAW invia instrument with an Ar laser source of 488 nm in a macroscopic configuration. The thermogravimetry/differential thermal analysis (TG-DTA) curves of Co@C under O_2 atmosphere was carried out with a TGA/DSC (METTLER TOLEDO) instrument at a heating rate of 10 °C/min. The samples were dried at 200 °C in air to remove the absorbed water before testing.

2.7. Electrochemistry

Electrochemical measurements were performed with a CHI 760 C electrochemical workstation in a 0.5 M H_2SO_4 aqueous solution. A Hg/Hg_2Cl_2 (saturated KCl, SCE) electrode and a carbon cloth were used as the reference and counter electrode, respectively. 5 mg of the catalyst powders was dispersed in 1 mL of 1:1 (v:v) water/ethanol mixed solvents along with 50 μL of a Nafion solution (5% Nafion in ethanol) , and the mixture was sonicated for 30 min. Then, 5 μL of the above solution was drop-cast onto the surface of a glassy carbon disk at a catalyst loading of 0.357 mg cm^{-2}. The as-prepared catalyst film was dried at room temperature. Polarization curves without ohmic compensation were acquired by sweeping electrode potentials from 0 to -0.8 V (vs. SCE) at a potential sweep rate of 5 mV s^{-1}. Electrochemical impedance spectroscopy (EIS) was carried out with frequency range from 100 kHz to 0.01 Hz. The main arc in the EIS spectra was fitted using a simplified Randles equivalent circuit, which consisted of a resistance (Rs, the total resistance from electrocatalyst, electrode, electrochemical workstation and electrolyte), a charge-transfer resistance (Rct, interface electrocatalytic reaction between electrode and electrolyte) and a constant phase element (CPE), and the fitting parameters were estimated through the application of the Levenberg–Marquardt minimization procedure. Cyclic voltammetry (CV) was used to probe the electrochemical double layer capacitance at non-faradaic potentials as a means to estimate the effective electrode surface area. Accelerated stability tests were performed in 0.5 M H_2SO_4 at room temperature by potential cycling between 0 and -0.5 V (vs. SCE) at a sweep rate of 100 mV s^{-1} for 1000 cycles. Current-time responses were monitored by chronoamperometric measurements at -0.15 V vs. RHE for 20 h.

0.027 mg of the electrocatalyst was deposited onto a carbon cloth electrode (1×1 cm^2) and i-*t* tests were carried out at the overpotential of 150 mV. The electrolytic tank was sealed by sealing film and the gas mixture of hydrogen and oxygen was

accumulated with the reaction time and collected by a micro-syringe every five min. The hydrogen and oxygen have the different peak positions in gas chromatography (GC-2060) due to the different molecular weights. The H_2 production was calculated according to the formula $V_{H2}=S_t/S_s \times V/(22.4 \times t)$, where S_t was the peak area of H_2 tested by GC for 1 mL gas collected from the sealed cell, S_s was the peak area tested by 1 mL pure hydrogen (99.9%), V was the volume of the electrolytic tank minus that of the electrolyte, and t was the test time.

3. Results and discussion

The etching process of metal@carbon by pre-oxidation was shown in Scheme 1a. The thermogravimetry/differential thermal analysis (TG-DTA) showed that the oxidation reaction of Co@C started at 330 °C and accelerated at 360 °C under O_2 atmosphere (Fig. 1). So, the O_2 etching temperature of Co@C was determined at 350 °C. The TG results of Co@C at 350 °C for different etching time of 1 h, 2 h and 3 h showed the negligible changes of carbon contents (1.1 – 2.5 wt%, Fig. S2), implying that the oxidation reaction mainly introduced more defects into carbon nanotubes, instead of forming CO_2 because the etching temperature was lower than the combustion temperature of carbon nanotubes (Fig. S3). After introducing the more defects into carbon nanotubes, the diffusion process and phase transformation of Co@C were easy to be achieved. According to the above reaction mechanism, the three-step synthetic process of

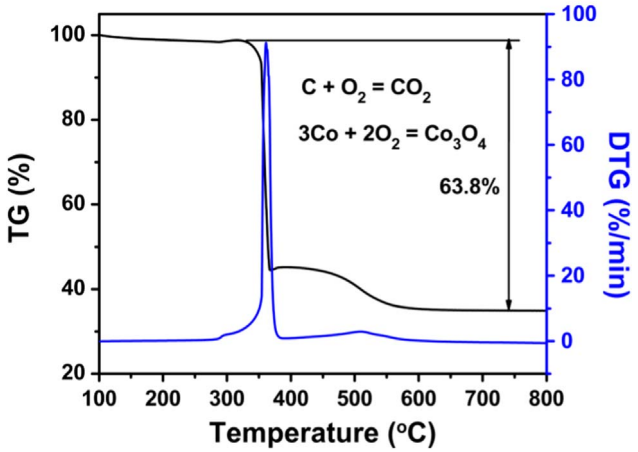

Fig. 1. TG-DTA curves of Co@C under O_2 atmosphere.

$CoSe_2$@DC, carbonization-oxidation-selenylation, was illustrated in Scheme 1b. Firstly, the polyhedral ZIF-67 as the precursor (Fig. S1a and S4) were calcined under an Ar atmosphere to form Co nanoparticles embedded carbon (Co@C), which possessed a rough surface and irregular morphology (Figs. S5a and S6a and b). Secondly, Co@C was oxidized in air at 350 °C to form Co_3O_4@DC (Figs. S5b and S6c and d). Finally, Co_3O_4@DC was further transformed to $CoSe_2$@DC through a selenylation process. It is worth mentioning that

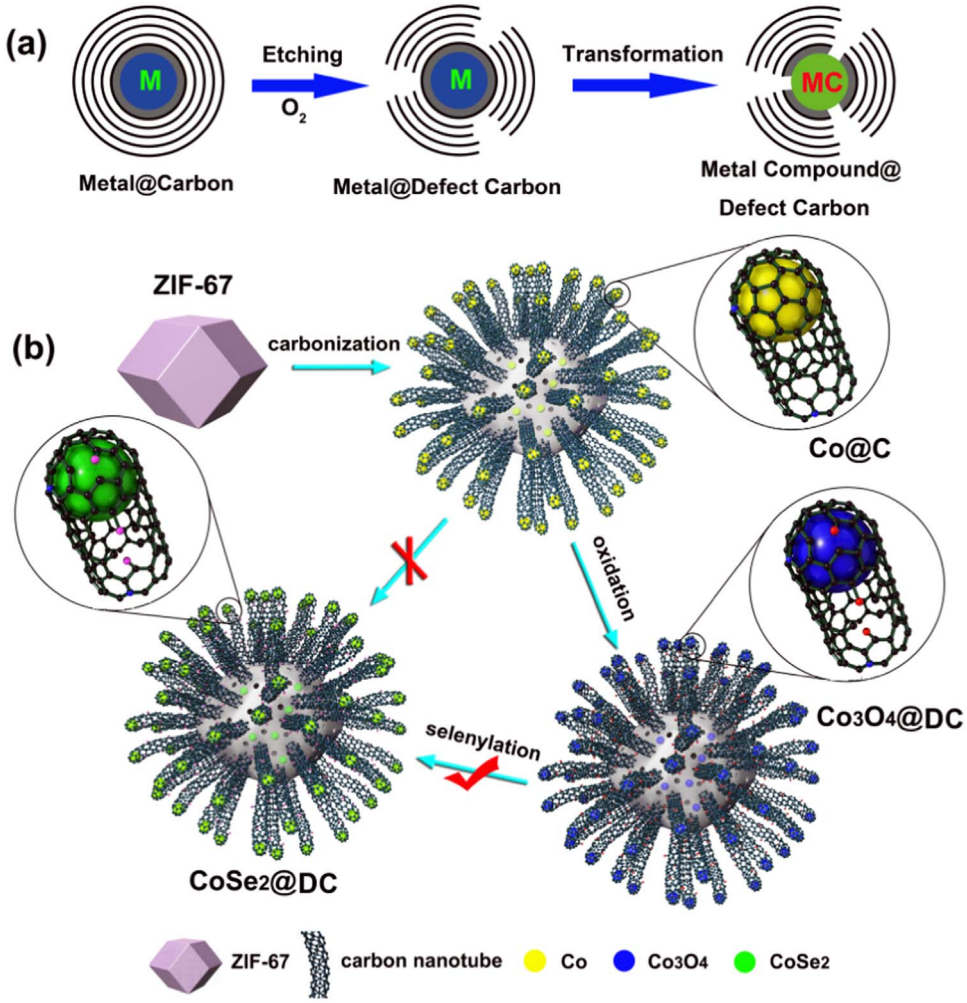

Scheme 1. Schematic illustration of (a) the etching process of metal@carbon by pre-oxidation and (b) the synthetic procedure for $CoSe_2$@DC.

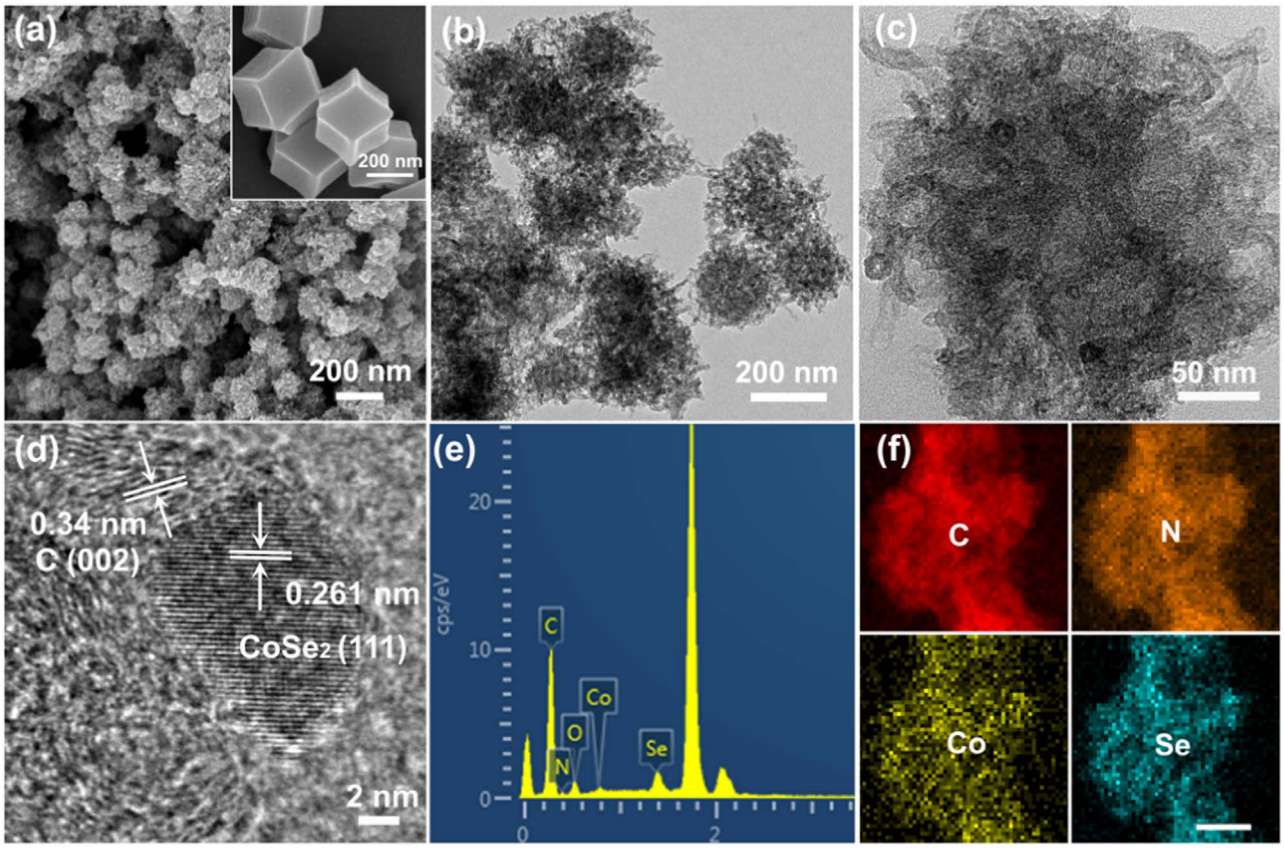

Fig. 2. (a) FESEM image, (b-d) TEM images and (e) EDX spectra of $CoSe_2$@DC. (f) The elemental mapping for C, N, Co, Se in $CoSe_2$@DC, the bar scale was 100 nm. Inset of Fig. 1a is the ZIF-67.

$CoSe_2$@DC can not be synthesized by direct selenylation of Co@C without pre-oxidation.

$CoSe_2$@DC possessed uniform morphology with an average size of ~300 nm and the surface was surrounded by various nanotubes (Fig. 2a). Transmission electron microscopy (TEM) further disclosed that $CoSe_2$@DC was composed of $CoSe_2$ nanoparticles embedded in carbon nanotubes (Fig. 2b and c). The diameters of carbon nanotubes were ~10 nm, similar to literature results [21], but smaller than that derived from the Co-dicyandiamide system [18,28]. High resolution transmission electron microscopy (HRTEM) image in Fig. 2d showed that a $CoSe_2$ nanoparticle with a size of ~10 nm was wrapped by a few carbon layers. There were two lattice fringes in $CoSe_2$@DC, 0.261 nm in the core and 0.34 nm in the shell, corresponding to (111) of $CoSe_2$ and (002) of graphic carbon, respectively. Energy-dispersive X-ray (EDX) analysis (Fig. 2e) confirmed the presence of C, N, Co, Se elements in $CoSe_2$@DC, and the corresponding elemental mapping (Fig. 2f) showed that Co and Se as discrete particles were embedded in the uniform distribution of C and N.

X-ray diffraction (XRD) measurements confirmed the success of the carbonization-oxidation-selenylation process in making the hybrid materials (Fig. 3a). The broad characteristic peak at 26° for graphic carbon appeared in all samples of Co@C, Co_3O_4@DC, $CoSe_2$@DC and Co@C-Se. However, the (002) peak intensities of graphic carbon became weaker after the pre-oxidation treatment, suggesting that pre-oxidation treatment destroyed the ordered structure of carbon. Raman spectra results also attested the above conclusion (Fig. 3b) and the characteristic D band (disordered carbon) and G band (graphic carbon) were observed. Comparing with Co@C (0.98), the higher I_D/I_G values of Co_3O_4@DC (1.19) also implied that more defects were introduced by pre-oxidation into carbon nanotubes (Table 1). In addition, the phase transformation of Co, Co_3O_4 and $CoSe_2$ was also confirmed by XRD. Before the pre-oxidation, only metal cobalt was detected in Co@C (JCPDS no. 15-0806). After pre-oxidation, Co_3O_4 was observed in the XRD pattern of Co_3O_4@DC (JCPDS no. 65-3103), consistent with Raman spectra results (Fig. 3b). Then, after selenylation, $CoSe_2$ was successfully synthesized (JCPDS no. 53-0449, Fig. S7). As a comparison, Co@C without pre-oxidation was directly selenided (Co@C-Se), and no $CoSe_2$ was detected in the XRD patterns. So, the pre-oxidation treatment as the crucial step introduced more defects into carbon, leading to higher reactivity.

X-ray photoelectron spectroscopy (XPS) was applied to further investigate the transformation process (Table 1). For Co@C, the Co 2p electrons yielded a peak at 778.3 eV, corresponding to metal Co. After oxidation, the content of O element increased up to 8.3 at% (Fig. 3c). Meanwhile, the peak with binding energy of 780.2 eV was corresponding to the Co $2p^{3/2}$ of Co_3O_4 phase (Fig. 3d). After selenylation, the O atoms were replaced by Se atoms to form $CoSe_2$ and the content of O element decreased to 2.6 at% (Fig. S8). As a comparison, Co 2p electrons in Co@C-Se only possessed the characteristic peak of Co° at 778.3 eV, implying that it was difficult to transform Co@C into $CoSe_2$@DC without the pre-oxidation procedure.

The electrocatalytic activities of $CoSe_2$@DC for HER were tested in a three-electrode system in 0.5 M H_2SO_4. For comparison, controlled samples of DC, $CoSe_2$ and $CoSe_2$ loaded on DC ($CoSe_2$/DC) were successfully synthesized (Fig. S9). As shown in Fig. 4a, the onset potential of $CoSe_2$@DC was −40 mV vs. RHE (Fig. S10, the potential to achieve 0.5 mA cm^{-2}, and 10 mA cm^{-2} at 132 mV), which was markedly better than those of DC (−206 mV) and $CoSe_2$ (−189 mV), but still inferior to that of 20 wt% Pt/C (−6 mV). It's worth noting that the HER activity of $CoSe_2$@DC was also superior to that of $CoSe_2$/DC (−169 mV), suggesting that both the

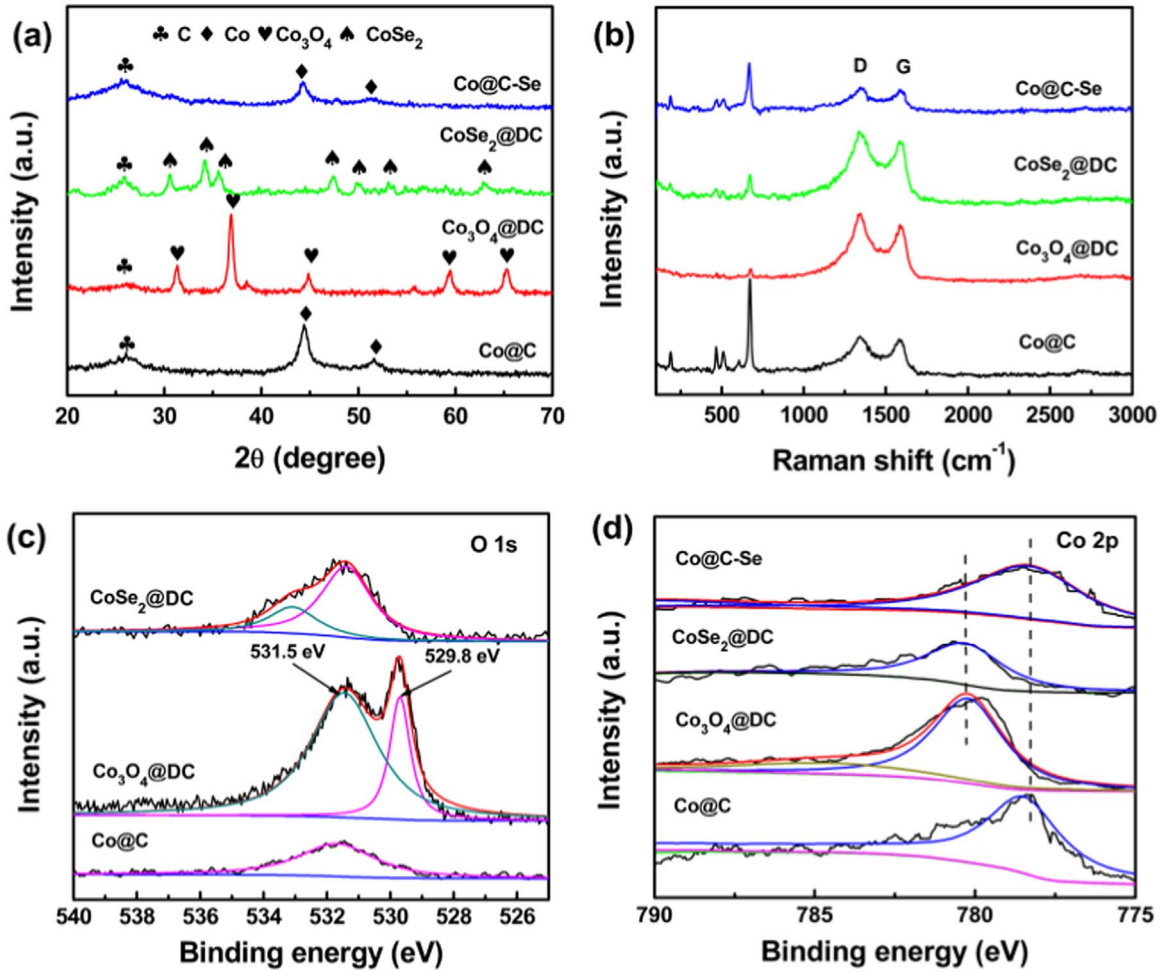

Fig. 3. (a) XRD patterns and (b) Raman spectra of Co@C, Co_3O_4@DC, $CoSe_2$@DC and Co@C-Se. High-resolution XPS spectrum of O 1 s (c) and Co 2p (d) for Co@C, Co_3O_4@DC, $CoSe_2$@DC and Co@C-Se.

Table 1
The comparison of Raman and XPS results for Co@C, Co_3O_4@DC, $CoSe_2$@DC and Co@C-Se, including I_D/I_G, component and valence state.

Samples	I_D/I_G	Component (at%)	Valence state of Co
Co@C	0.98	C (92.0), N (3.3), O (3.9), Co (0.8)	0
Co_3O_4@DC	1.19	C (87.6), N (3.3), O (8.3), Co (0.9)	+2/+3
$CoSe_2$@DC	1.04	C (88.7), N (4.4), O (2.6), Co (1.1), Se (3.2)	+2
Co@C-Se	1.05	C (89.1), N (6.4), Co (2.1), Se (2.4)	0

synergetic effect and core-shell structure played the important role in enhancing HER activity. In Fig. 4b, $CoSe_2$@DC also possessed a much smaller onset potential than those of Co_3O_4@DC (−179 mV), Co@C (−124 mV), and Co@C-Se (−114 mV). After the oxidation, the worse HER activity of Co_3O_4@DC was due to the oxidation state of Co [16]. The HER activity of Co@C-Se was also worse than that of $CoSe_2$@DC due to the unsuccessful phase transformation from Co to $CoSe_2$ Besides, the Se-doped carbon with the poor HER activity (−253 mV, Fig. S11) eliminated the doping effect on the enhanced HER activity.

Tafel slope revealed the inherent reaction processes of HER, and it can be calculated by the Tafel equation ($\eta = b \log j + a$, where j is the current density and b is the Tafel slope) (Fig. 4c). The Tafel slope value of $CoSe_2$@DC (82 mV dec^{-1}) was smaller than those of Co@C-Se (84.5 mV dec^{-1}), Co_3O_4@DC (89 mV dec^{-1}), $CoSe_2$/DC (98.4 mV dec^{-1}), DC (92.3 mV dec^{-1}), Co@C (83.3 mV dec^{-1}) and $CoSe_2$ (91.4 mV dec^{-1}) and indicated a Volmer–Heyrovsky mechanism for HER and the rate-limiting electrochemical desorption process. In fact, the metal@carbon electrocatalysts [29] usually possessed larger Tafel slope than those of transition metals based electrocatalysts (such as MoS_2, CoP, CoS_2) [30–32]. In addition, $CoSe_2$@DC also possessed a larger exchange current density of 0.5 mA cm^{-2} than those of $CoSe_2$ (0.005 mA cm^{-2}), $CoSe_2$/DC (0.325 mA cm^{-2}) and Co@C-Se (0.178 mA cm^{-2}). Further, the favorable kinetics was verified by electrochemical impedance spectroscopy (EIS, Fig. 4d). The charge transfer resistance (Rct) obtained from the semicircle in the low frequency zone is related to the electrocatalytic kinetics at the interface between electrocatalyst and electrolyte, and a lower value corresponds to a faster electron transfer [7,33,34]. $CoSe_2$@DC modified electrode possessed a Rct value of 30.1 Ω at a overpotential of 200 mV, which was much smaller than those of other electrocatalysts, suggesting a fast electron transfer and consequently facile HER kinetics at the electrocatalyst/electrolyte interface. Inset of Fig. 4d showed that the Rct values of $CoSe_2$@DC decreased rapidly with the increased overpotentials, from 114.6 Ω at $\eta = 150$ mV to 30.1 Ω at $\eta = 200$ mV.

The electrochemical area of $CoSe_2$@DC (51.1 mF cm^{-2}) estimated by cyclic voltammogram (CV) was larger than those of Co@C (39.5 mF cm^{-2}), Co_3O_4@DC (33.0 mF cm^{-2}), Co@C-Se (16.3 mF cm^{-2}) and $CoSe_2$/DC (11.4 mF cm^{-2}), as shown in Fig. S12 and Fig. 4**e**. The larger electrochemical area was associated with more active sites at the solid–liquid interface. However, after being corrected by electrochemical area, $CoSe_2$@DC still possessed the smallest onset potential (Fig. S13), implying that electrochemical

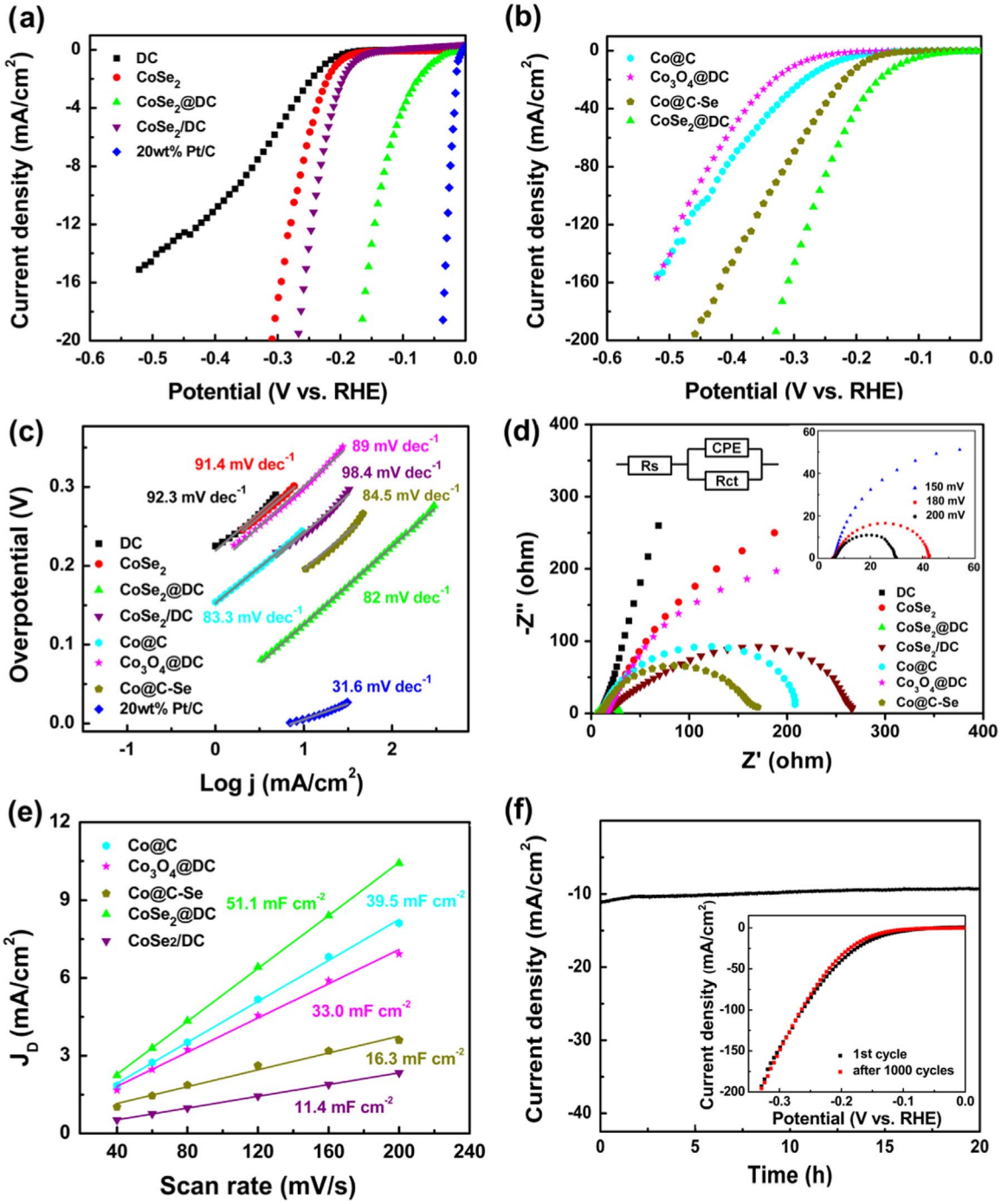

Fig. 4. (a) Polarization curves of DC, $CoSe_2$, $CoSe_2$/DC, $CoSe_2$@DC and 20 wt% Pt/C without iR correction. (b) Polarization curves of Co@C, Co_3O_4@DC, $CoSe_2$@DC and Co@C-Se. (c) the Tafel plots from (a, b). (d) Nyquist plots of the different samples modified electrodes with same overpotential of 200 mV. The inset was the equivalent circuit and Nyquist plots of $CoSe_2$@DC-modified electrodes with different overpotentials. (e) The capacitive currents as a function of scan rates. (f) Chronoamperometric response for $CoSe_2$@DC. The inset was the polarization curves of $CoSe_2$@DC before and after 1000 cycles.

area can only affect the catalytic current density, rather than the intrinsic catalytic activity of catalysts.

As shown in Fig. 4f, both the continuous amperometric i-t testing for 20 h and the polarization curves after 1000 cycles of CV suggested that $CoSe_2$@DC possessed the long-term extraordinary durability. The bubbles gathered on electrode surface was confirmed to be hydrogen by gas chromatography (Fig. S14), and the corresponding hydrogen production rate was 766.3 mmol g^{-1} h^{-1} (Fig. S15). The obtained Faradaic efficiency (FE) for $CoSe_2$@DC was nearly 100%, implying that $CoSe_2$@DC was an excellent HER electrocatalyst with the superior stability in acid media.

Such a HER performance of $CoSe_2$@DC (−40 mV vs. RHE, 82 mV dec^{-1}, exchange current density of 0.5 mA cm^{-2}) was better than or comparable to leading metal@carbon and transition metals-based HER powder catalysts. As shown in Table S1, $CoSe_2$@DC possessed the smallest onset potential, the smallest overpotential to achieve 10 mA cm^{-2} and the largest exchange current density among $CoSe_2$-based electrocatalysts. However, the Tafel slope of $CoSe_2$@DC was larger than those of $CoSe_2$-based electrocatalysts, but close to those of metal@carbon electrocatalysts. The excellent HER activity as well as extraordinary stability of $CoSe_2$@DC can be attributed to the following factors.

(i) The multilevel structure composed of carbon nanotubes derived from Co-MOF leading to a large electrochemical surface area with more active sites for HER (Fig. 4e). (ii) The novel structure, $CoSe_2$ nanoparticles partially embedded into defective carbon nanotubes, was proposed in Scheme 1. On the one hand, the active sites of $CoSe_2$ nanoparticles can be exposed in the electrolyte and contributed to HER [35]. On the other hand, the electronic density states of carbon were modulated by nonmetal doping [36] and transition-metal compounds [28,37,38], which introduced the additional catalytic activities of carbon shell.

4. Conclusions

In summary, an efficient electrocatalyst ($CoSe_2$@DC) derived from Co-based MOFs was successfully synthesized by the three-step carbonization-oxidation-selenylation procedure. The pre-oxidization was a crucial step for both the diffusion process of selenium atoms to form $CoSe_2$@DC and the introduction of defects into carbon nanotubes to expose catalytic sites of $CoSe_2$. The $CoSe_2$@DC composed of $CoSe_2$ nanoparticles as core were partially embedded defective carbon nanotubes showed excellent HER activity with a low onset potential of -40 mV vs. RHE with a Tafel slope of 82 mV dec^{-1}, a high current density (132 mV, 10 mA cm^{-2}) and robust stability in 0.5 M H_2SO_4. Herein, the reported pre-oxidization strategy of metal@carbon can expose active sites of the core, meanwhile, and maintain the porous carbon skeleton, which hold great potential for more applications in the electrocatalytic reactions.

Acknowledgments

This work was supported by the National Recruitment Program of Global Experts, Zhujiang New Stars of Science & Technology (2014J2200061), Project of Public Interest Research and Capacity Building of Guangdong Province (2014A010106005), the Fundamental Research Funds for the Central Universities (D2153880) and the National Natural Science Foundation of China (51502096).

Appendix A. Supporting information

Supplementary data associated with this article can be found in the online version at http://dx.doi.org/10.1016/j.nanoen.2016.08.040.

References

[1] Q. Gong, L. Cheng, C. Liu, M. Zhang, Q. Feng, H. Ye, M. Zeng, L. Xie, Z. Liu, Y. Li, ACS Catal. 5 (2015) 2213–2219.
[2] Z. Xing, Q. Liu, A.M. Asiri, X. Sun, Adv. Mater. 26 (2014) 5702–5707.
[3] M. Zeng, Y. Li, J. Mater. Chem. A 3 (2015) 14942–14962.
[4] M.S. Faber, S. Jin, Energy Environ. Sci. 7 (2014) 3519–3542.
[5] M.-R. Gao, J.-X. Liang, Y.-R. Zheng, Y.-F. Xu, J. Jiang, Q. Gao, J. Li, S.-H. Yu, Nat. Commun. 6 (2015) 5982.
[6] W. Zhou, D. Hou, Y. Sang, S. Yao, J. Zhou, G. Li, L. Li, H. Liu, S. Chen, J. Mater. Chem. A 2 (2014) 11358–11364.
[7] L. Liao, S. Wang, J. Xiao, X. Bian, Y. Zhang, M.D. Scanlon, X. Hu, Y. Tang, B. Liu, H. H. Girault, Energy Environ. Sci. 7 (2014) 387–392.
[8] W.F. Chen, C.H. Wang, K. Sasaki, N. Marinkovic, W. Xu, J.T. Muckerman, Y. Zhu, R.R. Adzic, Energy Environ. Sci. 6 (2013) 943–951.
[9] P. Jiang, Q. Liu, Y. Liang, J. Tian, A.M. Asiri, X. Sun, Angew. Chem. Int. Ed. 53 (2014) 12855–12859.
[10] E.J. Popczun, C.G. Read, C.W. Roske, N.S. Lewis, R.E. Schaak, Angew. Chem. 126 (2014) 5531–5534.
[11] W.-F. Chen, K. Sasaki, C. Ma, A.I. Frenkel, N. Marinkovic, J.T. Muckerman, Y. Zhu, R.R. Adzic, Angew. Chem. Int. Ed. 51 (2012) 6131–6135.
[12] B. Cao, G.M. Veith, J.C. Neuefeind, R.R. Adzic, P.G. Khalifah, J. Am. Chem. Soc. 135 (2013) 19186–19192.
[13] Y. Ito, W. Cong, T. Fujita, Z. Tang, M. Chen, Angew. Chem. 127 (2015) 2159–2164.
[14] Y. Zheng, Y. Jiao, L.H. Li, T. Xing, Y. Chen, M. Jaroniec, S.Z. Qiao, ACS Nano 8 (2014) 5290–5296.
[15] Y. Zhou, Y. Leng, W. Zhou, J. Huang, M. Zhao, J. Zhan, C. Feng, Z. Tang, S. Chen, H. Liu, Nano Energy 16 (2015) 357–366.
[16] W. Zhou, Y. Zhou, L. Yang, J. Huang, Y. Ke, K. Zhou, L. Li, S. Chen, J. Mater. Chem. A 3 (2015) 1915–1919.
[17] H. Liang, L. Li, F. Meng, L. Dang, J. Zhuo, A. Forticaux, Z. Wang, S. Jin, Chem. Mater. 27 (2015) 5702–5711.
[18] J. Deng, P. Ren, D. Deng, L. Yu, F. Yang, X. Bao, Energy Environ. Sci. 7 (2014) 1919–1923.
[19] W. Zhang, Z.-Y. Wu, H.-L. Jiang, S.-H. Yu, J. Am. Chem. Soc. 136 (2014) 14385–14388.
[20] W. Xia, R. Zou, L. An, D. Xia, S. Guo, Energy Environ. Sci. 8 (2015) 568–576.
[21] B.Y. Xia, Y. Yan, N. Li, H.B. Wu, X.W. Lou, X. Wang, Nat. Energy 1 (2016) 15006.
[22] H.B. Wu, B.Y. Xia, L. Yu, X.-Y. Yu, X.W.D. Lou, Nat. Commun. 6 (2015) 6512.
[23] Y. Hou, Z. Wen, S. Cui, S. Ci, S. Mao, J. Chen, Adv. Funct. Mater. 25 (2015) 872–882.
[24] J. Lu, W. Zhou, L. Wang, J. Jia, Y. Ke, L. Yang, K. Zhou, X. Liu, Z. Tang, L. Li, S. Chen, ACS Catal. 6 (2016) 1045–1053.
[25] Y. Hou, Z. Wen, S. Cui, S. Ci, S. Mao, J. Chen, Adv. Funct. Mater. 25 (2015) 872–882.
[26] M. Caban-Acevedo, M.L. Stone, J.R. Schmidt, J.G. Thomas, Q. Ding, H.-C. Chang, M.-L. Tsai, J.-H. He, S. Jin, Nat. Mater. 14 (2015) 1245–1251.
[27] W. Xia, Jh Zhu, Wh Guo, L. An, Dg Xia, Rq Zou, J. Mater. Chem. A 2 (2014) 11606–11613.
[28] X. Zou, X. Huang, A. Goswami, R. Silva, B.R. Sathe, E. Mikmeková, T. Asefa, Angew. Chem. 126 (2014) 4461–4465.
[29] X. Zheng, J. Deng, N. Wang, D. Deng, W.H. Zhang, X. Bao, C. Li, Angew. Chem. Int. Ed. 53 (2014) 7023–7027.
[30] Y. Li, H. Wang, L. Xie, Y. Liang, G. Hong, H. Dai, J. Am. Chem. Soc. 133 (2011) 7296–7299.
[31] M.A. Lukowski, A.S. Daniel, F. Meng, A. Forticaux, L. Li, S. Jin, J. Am. Chem. Soc. 135 (2013) 10274–10277.
[32] J. Tian, Q. Liu, A.M. Asiri, X. Sun, J. Am. Chem. Soc. 136 (2014) 7587–7590.
[33] J.J. Duan, S. Chen, B.A. Chambers, G.G. Andersson, S.Z. Qiao, Adv. Mater. 27 (2015) 4234–4241.
[34] L. Liao, J. Zhu, X.J. Bian, L. Zhu, M.D. Scanlon, H.H. Girault, B.H. Liu, Adv. Funct. Mater. 23 (2013) 5326–5333.
[35] D. Kong, H. Wang, Z. Lu, Y. Cui, J. Am. Chem. Soc. 136 (2014) 4897–4900.
[36] S.S. Shinde, A. Sami, J.-H. Lee, J. Mater. Chem. A 3 (2015) 12810–12819.
[37] J. Duan, S. Chen, M. Jaroniec, S.Z. Qiao, ACS Catal. 5 (2015) 5207–5234.
[38] H. Fei, J. Dong, M.J. Arellano-Jiménez, G. Ye, N.D. Kim, E.L. Samuel, Z. Peng, Z. Zhu, F. Qin, J. Bao, Nat. Commun. 6 (2015) 8868.

Dr. Weijia Zhou completed his pH.D. at Shandong University in 2012. He was doing research at Nanyang Technological University (NTU) in 2011. Now, Dr. Zhou is an associate professor in New Energy Research Institute, School of Environment and Energy, South China University of Technology (SCUT), China. His research interests are related to the design and synthesis of functional materials and devices for new energy conversion and storage, including photo and electro-catalytic water splitting, CO_2 reduction and supercapacitor.

Jia Lu received her B.S. degree at South China Agriculture University in 2013, and now she is a master degree candidate at South China University of Technology (SCUT) under the supervision of Dr. Weijia Zhou and Prof. Shaowei Chen. Her research interest includes metal embedded carbon hybrid catalysts for oxygen reduction reaction and electrochemistry of water splitting.

Kai Zhou is currently pursuing a PhD under the supervision of Dr. Weijia Zhou and Prof. Shaowei Chen in the School of Environment and Energy at the South China University of Technology, China. His research is focused on the designs and synthesis of nanomaterials for energy conversion and storage.

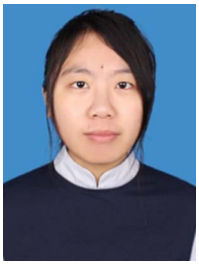

Linjing Yang received B.S. degree from Hebei University of Technology in 2014. She is pursuing her M.D. degree under the supervision of Dr. Weijia Zhou and Prof. Shaowei Chen in New Energy Research Institute, South China University of Technology (SCUT). Her research interests include electrocatalytic water splitting and oxygen reduction.

Yunting Ke has been studying in College of Environment and Energy, South China University of Technology (SCUT), since 2013. She is doing experiments under the supervision of Dr. Weijia Zhou in New Energy Research Institute. Her research interest is electro-catalytic water splitting.

Dr. Zhenghua Tang currently is an associate professor of New Energy Research Institute at South China University of Technology. He is also the recipient of Guangdong Natural Science Funds for Distinguished Young Scholar. He obtained his B. S. degree at Lanzhou University in 2005. He started his PhD program since August 2007 in Department of Chemistry, Georgia State University, USA. After that, he conducted his postdoctoral training at Department of Chemistry, University of Miami from 2012 to 2014. He started his current position since August 2014. His research focuses on noble metal nanoclusters, nanocatalyst, electrochemistry, and peptide based nanomaterials.

Dr. Shaowei Chen obtained a B.Sc. degree from the University of Science and Technology of China, and then went to Cornell University receiving his M.Sc. and pH.D. degrees in 1993 and 1996. Following a postdoctoral appointment in the University of North Carolina at Chapel Hill, he started his independent career in Southern Illinois University in 1998. In 2004, he moved to the University of California at Santa Cruz and is currently a Professor of Chemistry. He is also an adjunct professor at South China University of Technology. His research interest is primarily in the electron transfer chemistry of nanoparticle materials.